Calculation of the velocities induced by the trailing vorticity in the rotor plane of a horizontal-axis turbine or propeller

David H. Wood*

Department of Mechanical and Manufacturing Engineering, University of Calgary, Calgary, AB, Canada

Lifting line (LL) analysis of propellers and horizontal-axis turbines requires the axial and circumferential velocities induced by the vortex system representing the blades and the trailing vorticity. If the blades are straight and radial, the induced velocities along the LLs are due only to the trailing vorticity. Accurate two-term approximations for these velocities have been developed from the exact Kawada–Hardin (KH) equations for the velocity field of a doubly infinite helical vortex of constant pitch and radius, Wood et al. (Ocean Engineering, 2021, 235). This paper describes a straightforward extension of the approximations to give the induced velocities anywhere in the equivalent of the rotor plane for a doubly infinite helix. The third term in the approximation of the KH equations is derived and compared to an alternative third term due to Okulov (Journal of Fluid Mechanics, 2004, 521, 319–342). Both three-term approximations produce a small improvement in accuracy over the two-term approximations for a range of operating conditions for turbines and propellers. Okulov's third term is superior. To determine the induced velocities for a singly infinite trailing vortex behind a rotor, an additional equation is derived from the Biot–Savart law. Numerical examples show that the resulting equations provide accurate estimates for the induced velocities over the rotor plane. The main application of the analysis is to account for blade sweep and coning by including the angle between the vortex origin and the control point at which the velocities are required, often the center of each blade element.

KEYWORDS

wind turbine aerodynamics, blade element, momentum (BEM) theory, vortex dynamics, helical vortex, Kawada–Hardin equations, Biot–Savart law

1 Introduction

This study extends the analysis by Wood et al. (2021) of the velocities induced at the blades by the helical trailing vortices for lifting line (LL) analysis of horizontal-axis turbines and propellers. Wood et al. (2021) considered only identical, straight, equispaced blades that lie in the radial plane of rotation. The vortices were assumed to have constant pitch

Abbreviations: BEMT, blade element/momentum theory; BS, Biot–Savart; KH, Kawada–Hardin; LL, lifting line; O, Okulov; W, Wrench.

and radius as this is the only case with closed-form expressions for the induced velocities. The restriction of constant pitch is not significant as Wood and Hammam (2022) showed that the pitch is constant throughout the wake of optimal rotors as it is the ratio of torque to thrust. The restriction of constant radius is possibly more significant, but at least, the constant radius analysis captures the important features of circumferential periodicity for identical, equispaced blades. Some further comments on the effects of wake expansion and radial velocity are made in Subsection 2.1. Wood et al. (2021) surveyed the approximate methods to compute the velocities along a straight LL based on the exact Kawada–Hardin (KH) equations described in Section 2.1. There are, however, situations that involve the induced velocities throughout the rotor plane rather than just along straight LLs. An example is a swept rotor, with the LL curved in the plane of rotation, which has been the subject of a significant amount of recent research, e.g., Fritz et al. (2022), Li et al. (2022b), and Gemaque et al. (2022). The first two studied swept wind turbine blades using different approximations for the induced velocities. Fritz et al. (2022) used a restricted version of the analysis developed here, whereas Li et al. (2022b) used a vortex-cylinder model of the wake. It is suggested that the present analysis is simpler and more general. Gemaque et al. (2022) investigated blade sweep for a hydrokinetic turbine without explicit incorporation of the spatial dependence of the induced velocities. In other words, they used Prandtl's well-known tip loss factor in their blade element/momentum theory (BEMT) calculations. Bergmann et al. (2021) analyzed propeller performance also using BEMT and Prandtl's tip loss factor. A possibly more important example is a coned rotor (Li et al., 2022a). Most modern large blades have pre-bend; the tips are upwind of the hub at a low wind turbine. As the wind speed and aerodynamic loads increase, the blades deflect downwind out of the radial plane of rotation due to their inherent flexibility. No study of coned rotors has considered the effect on the induced velocities of any axial displacement between the start of a trailing vortex and the control point where the induced velocity is required.

Figure 1 shows a doubly infinite helical vortex whose velocity field is given by the KH equations. When the angle θ in the figure is zero, the velocity induced along the LL by the singly infinite blue vortex shed at radius t, also along the LL, is one-half the doubly infinite value and so follows immediately from the KH equations. The present analysis accounts for a non-zero θ between the start of each trailing helical vortex and the control point, often the center of a blade element. Note that the terms "trailing" and "singly infinite" are synonymous. It will be shown that non-zero θ requires more than the KH equations. Initially, the blades are assumed to remain in the plane of rotation, and the extension to coned blades will be outlined subsequently as a small extension of the analysis.

The next section describes the KH equations and their two-term approximations for the velocities along the LLs and the new extension to the whole rotor plane. Then, the third-order approximations are derived and compared to those due to Okulov (2004) and Okulov and Sørensen (2020), which they called "remainders." The testing of the accuracy of the approximations is described in Section 3; the remainders are generally more accurate than the third-order corrections. As mentioned above, a major complication is that the KH equations apply to a doubly infinite helical vortex, whereas the velocities at $x = 0$ are needed for the

trailing blue vortex in Figure 1. When $\theta = 0$, the singly infinite induced velocities are one-half the doubly infinite ones; it is shown at the start of Section 4 that the doubly infinite results for non-zero θ give the sum of the induced velocities at $\pm\theta$ for a trailing vortex, and a further relation between these velocities is needed. Section 4 continues by using the Biot–Savart law to derive an approximate further relation for the difference in the velocities at $\pm\theta$. Section 5 describes numerical tests of the singly infinite equations. Section 6 discusses the results, shows how the analysis can be extended to coned rotors, and contains the conclusions. Appendix A describes the derivation of the sums needed for the $\theta-$ dependent approximations, and Appendix B shows the three terms in the approximation integration to zero over the region of planar symmetry as a check on the consistency of the derivation. Appendix C presents the analytic remainders added to the numerical integral of the Biot–Savart law for the singly infinite helices.

2 The equations for the velocities induced by doubly infinite helices

2.1 The exact equations

Cylindrical polar coordinates are used: (x, r, θ), where x is in the axial or streamwise direction, r is the radius, and θ is the circumferential angle. The respective velocity components are (u, v, w). A doubly infinite helical vortex of constant pitch p, defined by $dx/d\theta = p$ for any point on the vortex, passes through $(0, t, 0)$, as shown in Figure 1. The vortex radius remains t throughout the wake. u at any point $(0, r, \theta)$ along straight and radial LLs is given by the KH equations, Kawada (1936), Kawada (1939), and Hardin (1982), as described, for example, in Wood et al. (2021):

$$u(r,\theta) = \overline{u}(r) + u'(r,\theta) = \begin{cases} \dfrac{\Gamma}{2\pi p} - \dfrac{\Gamma t}{\pi p^2} S_1 & \text{if } r < t, \\ \\ -\dfrac{\Gamma t}{\pi p^2} S_3 & \text{if } r > t. \end{cases} \quad (1)$$

Here, Γ is the vortex strength, and the overline indicates a circumferentially averaged value. Similarly, the circumferential velocity, w, is given by

$$w(r,\theta) = \overline{w}(r) + w'(r,\theta) = \begin{cases} \dfrac{\Gamma t}{\pi p r} S_1 & \text{if } r < t, \\ \\ \dfrac{\Gamma}{2\pi r} + \dfrac{\Gamma t}{\pi p r} S_3 & \text{if } r > t. \end{cases} \quad (2)$$

Note that the mean velocity only appears for $r < t$ in Eq. 1 and for $r > t$ in (2). Thus, only the vortices above a blade element contribute to its mean axial velocity, and only those below it, to the mean circumferential velocity. Furthermore, the perturbation velocities determined by S_1 and S_3 are directly related by "helical symmetry": $pu'(r,\theta) = -rw'(r,\theta)$, which simplifies their computation. It is noted that helical symmetry also relates $\overline{u}(r,\theta)$ to $\overline{w}(r,\theta)$, but its demonstration relies on Kelvin's theorem for the strength of the vortices trailing from the top and bottom of each blade element and
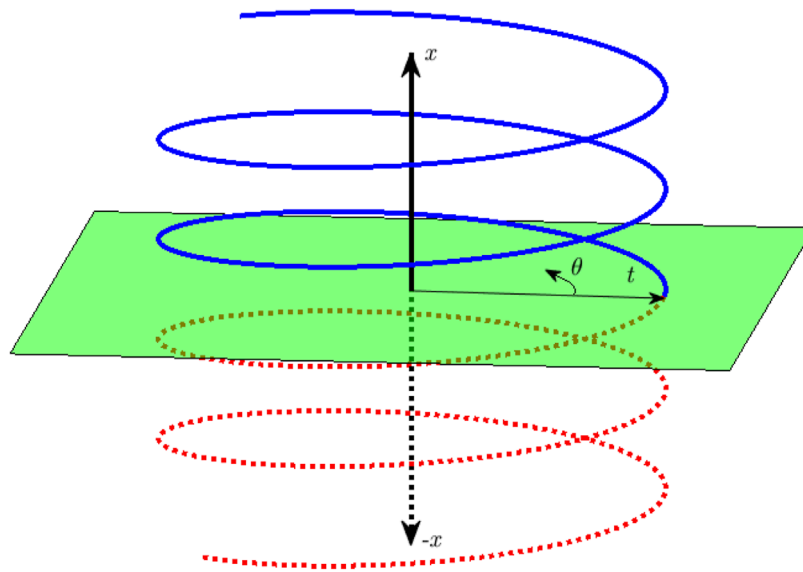
FIGURE 1
A doubly infinite helical vortex of constant pitch (p, not shown) and radius (t) extends from $+\infty$ to $-\infty$. The negative x–axis and vortex for negative x are shown as dashed lines. The first aim of the present work is to extend the analysis that gives the induced velocities in the green plane for any radius (r), but $\theta = 0$ only to any (r, θ). $\theta = 0$ is defined by the intersection of the vortex and the green plane. The induced velocities, (u, v, w), are in the (x, r, θ) directions.

is not needed here. As noted above, Eqs (1) and (2) apply to a doubly infinite vortex. The series S_1 and S_3 in the notation of Hardin (1982) are given by

$$S_1 = \sum_{m=1}^{\infty} m K'_m (mt/p) I_m (mr/p) \cos(m\theta) \qquad (3)$$

and

$$S_3 = \sum_{m=1}^{\infty} m I'_m (mt/p) K_m (mr/p) \cos(m\theta). \qquad (4)$$

Here, $I_m(.)$ and $K_m(.)$ are modified Bessel functions in standard notation. m denotes the order and the prime a derivative with respect to the argument. In practice, the derivatives are evaluated using the standard results $I'_m(.) = (I_{m-1}(.) + I_{m+1}(.))/2$ and $K'_m(.) = -(K_{m-1}(.) + K_{m+1}(.))/2$.

S_1 and S_3 completely determine both u and w, which are the focus of this study. The induced radial velocity, v, is generally ignored in BEMT, but this may not be justified for coned and swept rotors if the radial flow over the blade elements alters the element's lift and drag. v may also be important for any rotor with significant expansion of the wake as u and v have the same magnitude for any swept or unswept rotor and any wake expansion (Limacher and Wood, 2021). There are two main problems in extending the present analysis to v. The first is that a significant v implies a significant variation in the vortex radius, t, for which no analytic solutions are known. Second, the series for v when t is constant, S_2 and S_4 in the notation of Hardin (1982), involve products of $I'_m(.)$ and $K'_m(.)$ and would need extra analysis to produce the rotor plane approximations. v is not considered further in this study. Note that the terms involving S_1 and S_3 give the perturbations from the streamtube averages. The perturbations must integrate to zero over the azimuthal region of symmetry, $2\pi/N$, where N is the number of

blades. This constraint will be used later to check the approximate equations for u' and w'.

Clearly, Γ must be known to convert S_1 and S_3 into induced velocities. In the BEMT, Γ is the difference in the bound circulation of the elements on either side of the trailing vortex whose induced velocity is being calculated. Γ is easily determined from the element lift and drag, but this determination is outside the scope of the present work. All other parameters for the induced velocities are set by the rotor geometry, except for p. It can be calculated from the blade element thrust and torque, or equivalently, from $\overline{u}$ and $\overline{w}$ immediately behind the blades (Wood and Hammam, 2022).

Wood et al. (2021) analyzed methods to find u and w at $x = \theta = 0$ due to a vortex also starting at $x = \theta = 0$. This restricted the analysis to straight, radial blades. Removing this restriction is the purpose of the present analysis, which is made easier by the dependence of S_1 and S_3 on θ being separate from that on the coordinates and length parameters. Thus, each term in the Kapteyn-like series of products of Bessel functions and their derivatives in S_1 and S_3 can be summed over the N blades before summing the series in m, as explained by Wood et al. (2021). The circumferential summation is exact only if the blades are identical and equispaced, which can hold for swept and straight blades and will be assumed here. Summing over the N blades introduces what Wood et al. (2021) called "Kawada" cancellation: the original 2π azimuthal periodicity of a single trailing vortex becomes a $2\pi/N$ periodicity of N identical vortices, and this cancels a fraction of $(N-1)/N$ of the terms in the sums.

With Kawada cancellation, S_1 and S_3 reduce to

$$S_1 = N \sum_{m=1}^{\infty} m N K'_{mN} (mNt/p) I_{mN} (mNr/p) \cos(mN\theta) \qquad (5)$$

and

TABLE 1 Correspondence of the present symbols to Wrench (1957).

Present	Wrench (1957)
N	g
m	n
n	m
r/p	y
t/p	y_0

$$S_3 = N \sum_{m=1}^{\infty} mNI'_{mN}(mNt/p) \, K_{mN}(mNr/p) \cos(mN\theta). \quad (6)$$

All further references to S_1 and S_3 are to these equations for N blades which, obviously, include $N = 1$ as a special case.

Kawada cancellation removes two-thirds of the terms if $N = 3$, but the exact series for the induced velocities remains numerically challenging, partly because the number of terms required for a specified accuracy increases without bound as $r \to t$. Wood et al. (2021) described the considerable historical effort to develop accurate approximate equations. The next section describes those of Wrench (1957), which were shown by Wood et al. (2021) to be the most accurate two-term approximations.

2.2 Wrench's approximate equations

Wrench used the asymptotic expansion of $I_m(.)$ by Lehmer (1944) and his own, a similar expansion of $K_m(.)$. Eq. 19 of Wrench (1957) gives the $m-$th term in S_1 for $\theta = 0$, in the present notation, as

$$mNK'_{mN}(mNt/p) \, I_{mN}(mNr/p)$$
$$\sim -AU_W^m\left(1 + \frac{(t/p)^2}{2mNc_t^3}\right)\exp\left(\frac{\psi_1\left((r/p)^2\right)}{mNc_r^3} - \frac{\psi_1\left((t/p)^2\right)}{mNc_t^3}\right), \quad (7)$$

where the parentheses show only the first two terms that Wrench retained in each expansion. In (7),

$$A = \frac{p}{2t}\sqrt{\frac{c_t}{c_r}}, \text{ where } c_t = \sqrt{1 + (t/p)^2}, c_r = \sqrt{1 + (r/p)^2}, \text{ and}$$

$$U_W = \left[\frac{t(c_r - 1)}{r(c_t - 1)}\exp(c_r - c_t)\right]^N. \quad (8)$$

The function ψ_1 is defined as

$$\psi_1\left(z^2\right) = (3z^2 - 2)/24 \quad (9)$$

for any z, from Wrench's Eq. 11. For readers interested in the details of the derivation of the induced velocities, Table 1 relates the variables used in the present analysis to Wrench's equations.

Wrench expanded the exponential term in (7) to the leading order in ψ_1 to yield

$$mNK'_{mN}(mNt/p) \, I_{mN}(mNr/p)$$
$$\sim -AU_W^m\left(1 + \frac{(t/p)^2}{2mNc_t^3}\right)\left(1 + \frac{3(r/p)^2 - 2}{24mNc_r^3} - \frac{3(t/p)^2 - 2}{24mNc_t^3}\right)$$
$$\sim -AU_W^m\left(1 + \frac{B}{mN}\right), \quad (10)$$

where

$$B = \frac{1}{24}\left[\frac{9(t/p)^2 + 2}{c_t^3} + \frac{3(r/p)^2 - 2}{c_r^3}\right]. \quad (11)$$

Note that A and B are independent of m and, for future purposes, θ. The approximation for each term in S_3 was developed analogously from Eq. 20 of Wrench (1957):

$$mNI'_{mN}(mNt/p) \, K_{mN}(mNr/p)$$
$$\sim AU_W^{-m}\left(1 - \frac{(t/p)^2}{2mNc_t^3}\right)\exp\left(\frac{\psi_1\left((t/p)^2\right)}{mNc_t^3} - \frac{\psi_1\left((r/p)^2\right)}{mNc_r^3}\right)$$
$$\sim AU_W^{-m}\left(1 - \frac{(t/p)^2}{2mNc_t^3}\right)\left(1 + \frac{3(t/p)^2 - 2}{24mNc_t^3} - \frac{3(r/p)^2 - 2}{24mNc_r^3}\right)$$
$$\sim AU_W^{-m}\left(1 - \frac{B}{mN}\right). \quad (12)$$

For both S_1, with $U_W < 1$, and S_3, with $U_W > 1$, the summation over $1 \le m < \infty$ is easy for the $A-$ term as it is a geometric series. Added to the sum of the second term derived in Appendix A, Wrench's approximations become

$$S_{1,W} = -A\left[\frac{NU_W}{1 - U_W} + B\log\left(1 + \frac{U_W}{1 - U_W}\right)\right] \quad (13)$$

for $r < t$ and

$$S_{3,W} = A\left[\frac{N}{U_W - 1} - B\log\left(1 + \frac{1}{U_W - 1}\right)\right] \quad (14)$$

for $r > t$, which are Eqs 15, 16 of Wood et al. (2021). It is clear from Eqs 13, 14 that $S_{1,W}$ and $S_{3,W}$ become singular as $r \to t$ and $U_w \to 1$. This is the situation mentioned above, which causes the unbounded increase in the number of terms in the Kapteyn series that must be summed to achieve a specified accuracy. A major advantage of the approximate solutions is that they remain accurate for any $U_W \ne 1$ (Wood et al., 2021).

Including θ in the approximations is straightforward. The second line of Eq. 10 becomes

$$mNK'_{mN}(mNt/p) \, I_{mN}(mNr/p)\cos(mN\theta)$$
$$\sim -AU_W^m\left(1 + \frac{B}{mN}\right)\cos(mN\theta), \quad (15)$$

and the same factor of $\cos(mN\theta)$ multiplies the right sides of (12). The results in Appendix A allow the generalization of Eqs 13, 14 to be

$$S_{1,W} = -A\left[N\frac{U_W(\cos(N\theta) - U_W)}{1 + U_W^2 - 2U_W\cos(N\theta)}\right.$$
$$\left. - \frac{B}{2}\log\left(1 + U_W^2 - 2U_W\cos(N\theta)\right)\right] \quad (16)$$

for $r < t$ and

$$S_{3,W} = A \left[N \frac{U_W \cos(N\theta) - 1}{1 + U_W^2 - 2U_W \cos(N\theta)} \right.$$
$$\left. + \frac{B}{2} \log \left(\frac{1 + U_W^2 - 2U_W \cos(N\theta)}{U_W^2} \right) \right] \quad (17)$$

for $r > t$. It will be shown in Section 3 that the second term, which will be called the "$B-$ term" despite it containing A, is typically small compared to the $A-$ term. Both terms become singular as $r \to t$ and $U_W \to 1$, but only when $\theta = 0$. This singularity is associated with the complex nature of the flow in the immediate vicinity of the vortex, e.g., Boersma and Wood (1999) and Okulov and Sørensen (2020), and does not appear to detract from the usefulness of the equations for computing the induced velocities for LL analysis.

2.3 Higher-order terms in Wrench's expansion

The next term in Wrench's expansion has not been derived previously in the open literature. It is now given for S_1, and the very similar result for S_3 will be quoted. Extending (10) gives

$$mNK'_{mN}(mNt/p) I_{mN}(mNr/p)$$
$$\sim -AU_W^m \left(1 + \frac{(t/p)^2}{2mNc_t^3} + \frac{(t/p)^2 (4 - (t/p)^2)}{8(mNc_t^3)^2} \right)$$
$$\exp \left[\sum_{n=1}^{2} \left(\frac{\psi_n((r/p)^2)}{(mNc_r^3)^n} + (-1)^n \frac{\psi_n((t/p)^2)}{(mNc_t^3)^n} \right) \right]$$
$$\sim -AU_W^m \left(1 + \frac{B}{mN} + \frac{C_W}{m^2 N^2} \right). \quad (18)$$

Since

$$\psi_2(z^2) = z^2(z^2 - 4)/16 \quad (19)$$

for any z, from Eq. 11 of Wrench (1957), C_W is obtained as

$$C_W = \frac{1}{16} \left[\frac{1}{c_r^6} \left(\frac{9(r/p)^4}{8} - \frac{25(r/p)^2}{6} + \frac{1}{18} \right) \right.$$
$$+ \frac{1}{c_r^3 c_t^3} \left(\frac{3(r/p)^2 (t/p)^2}{4} + \frac{(r/p)^2}{6} - \frac{(t/p)^2}{2} - \frac{1}{9} \right)$$
$$\left. - \frac{1}{c_t^6} \left(\frac{15(t/p)^4}{8} - \frac{9(t/p)^2}{2} - \frac{1}{18} \right) \right]. \quad (20)$$

Using the results from Appendix A, $S_{1,W}$ becomes

$$S_{1,W} = -A \left[N \frac{U_W (\cos(N\theta) - U_W)}{1 + U_W^2 - 2U_W \cos(N\theta)} \right.$$
$$- \frac{B}{2} \log(1 + U_W^2 - 2U_W \cos(N\theta))$$
$$\left. + \frac{C_W}{2N} \left\{ \mathrm{Li}_2 \left(U_W e^{iN\theta} \right) + \mathrm{Li}_2 \left(U_W e^{-iN\theta} \right) \right\} \right] \quad (21)$$

for $r < t$, and the extended $S_{3,W}$ for $r > t$ is

$$S_{3,W} = -A \left[N \frac{U_W \cos(N\theta) - 1}{1 + U_W^2 - 2U_W \cos(N\theta)} \right.$$
$$+ \frac{B}{2} \log \left(\frac{1 + U_W^2 - 2U_W \cos(N\theta)}{U_W^2} \right)$$
$$\left. + \frac{C_W}{2N} \left\{ \mathrm{Li}_2 \left(e^{iN\theta}/U_W \right) + \mathrm{Li}_2 \left(e^{-iN\theta}/U_W \right) \right\} \right]. \quad (22)$$

$\mathrm{Li}_2(.)$ in these equations is the dilogarithm function, described in chapter 25 of DLMF (2023). As mentioned above, S_1 and S_3 give the perturbations from the circumferential average velocities in the rotor plane. Because $A, B,$ and C are not related, the $A-$, $B-$, and $C-$ terms must individually integrate to zero over $[0, 2\pi/N]$. Appendix B shows this to be the case for all three, which provides a check on the derivation of the $\theta-$dependent terms.

2.4 Higher-order terms due to Okulov

Okulov (2004) and Okulov and Sørensen (2020) used an alternative strategy to the asymptotic expansion of the Bessel functions in S_1 and S_3. They separated "the key terms from the series" and developed remainders to improve the accuracy. Wood et al. (2021) showed the key terms are identical to Wrench's two-term approximations in Eqs 13, 14 for $\theta = 0$, and, by implication, to (16) and (17) for non-zero θ. Following the recommendation of Okulov and Sørensen (2020) to use only the first term in their Eq. (A6a), the alternative $C-$ term, $C_{1,O}$, for S_1 in the present notation is

$$C_{1,O} = \left(K'_1(t/p) I_1(r/p) + AU_O(1 + B) \right) \cos(\theta), \quad (23)$$

where $U_O = U_W$ for $N = 1$. Using (15), the leading term in $C_{1,O}$ is

$$C_{1,O} \sim -AU_O C \cos(\theta), \quad (24)$$

and for $S_{3,O}$ is

$$C_{3,O} \sim AC \cos(\theta)/U_O. \quad (25)$$

In the numerical experiments described in Section 3, the approximations, $S_{1,O}$ and $S_{3,O}$, are given in Eqs (21) and (22), respectively, with the $C-$ term replaced by either (24) or (25).

3 Numerical tests of the approximate doubly infinite equations

Wood et al. (2021) documented the range of pitch values for a number of simulations and experiments on wind and hydrokinetic turbines and propellers, which led them to choose representative values of $p = 0.1, 1$ and $N = 4$ for their numerical tests to determine the accuracy of the approximate equations for $\theta = 0$. The accuracy depends on N, but the dependence on p is stronger; decreasing p, which corresponds to increasing the tip speed ratio for turbines, increases the accuracy. Because of the close similarity between S_1 and S_3, only the former is considered here for $N = 3$. S_1 was calculated directly from Eq. 5 by summing to a maximum value of $m = m_{max}$, chosen to give an accuracy of 10^{-8} using Eq. 18 of Wood et al. (2021), which assumes $\theta = 0$. Since the Kapteyn series will converge more rapidly for $\theta \neq 0$, using an upper limit of $m_{max} \forall \theta$ should be safe. $S_{1,A}$ is the $A-$ term in the approximation, that is, the first term in (21), and $S_{1,W}$ includes all three terms.

The results shown in Figure 2 correspond to a tip speed ratio of approximately 7, and $t = 1$ and $r = 0.99$ represent the tip vortex and the center of the blade element at the tip, respectively, when the number of elements per blade is around 50. Since S_1 and S_3
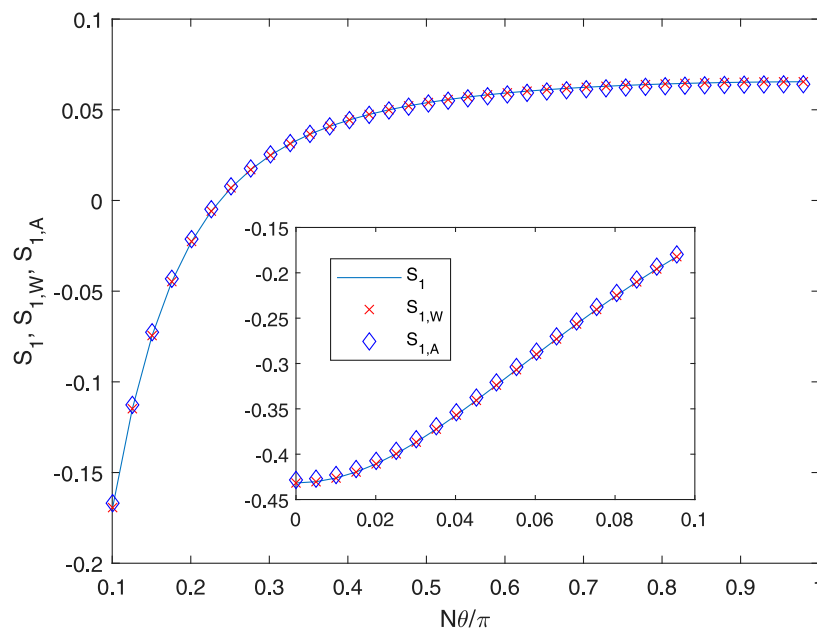
FIGURE 2
S_1, $S_{1,W}$, and $S_{1,A}$ for $p = 0.1$, $r = 0.99$, and $t = 1$.

are even in θ, 200 equispaced points over the positive region of symmetry, $\theta = [0, \pi]$, were computed, but only every fifth point is plotted in the main figure. The inset amplifies the region near $\theta = 0$ for all points in that region. For these conditions, $m_{max} = 59$, indicating the considerable computational burden of summing the exact equations. Wrench's approximation is very accurate; the r.m.s difference between S_1 and $S_{1,W}$ over the 200 points calculated for $0 \leq \theta \leq \pi/N$ was almost within the tolerance of calculating S_1. Using the $A-$ term only gives reasonable accuracy at $p = 0.1$. For $\theta = 0$, $S_1 = -0.43172$, $S_{1,A} = -0.42838$, and $S_{1,W} = -0.43172$; so using the first term only in the approximation gives a modest error of less than 1%.

It is inferred from these results that the $C-$ term or Okulov's alternative is not significant at this p. Their behavior is shown in Figure 3. Okulov's third term, Eq. 24, is more accurate than C_W from (21), but both could be used to determine the accuracy of using only two terms, i.e., Eqs 16, 17. Increasing p to $p = 1$ increases the time required for the evaluation of the exact solution. For the same N, t, and r, m_{max} becomes 519, and an accurate summation was not possible. r was decreased to 0.98, for which $m_{max} = 250$. The results are shown in Figures 4, 5. At $\theta = 0$, $S_1, S_{1,W}$, and $S_{1,A}$ were 1.7152, 1.7154, and 1.6933, respectively, all multiplied by 10^4. The accuracy of the approximations is slightly worse than that at $p = 0.1$, and Figure 5 shows that the two versions of the $C-$ term have become nearly equal. In particular, it is noted that the $A-$ term is a significantly poorer approximation to the exact solution at its higher p.

Other combinations of N, p, t, and r were investigated but not presented as the results shown are typical. The extension of Wrench's approximations for $\theta = 0$ to any θ was found to be accurate for a representative range of the parameters, and the accuracy can be improved and/or assessed by the $C-$ term or Okulov's alternative.

4 The velocities induced by a singly infinite vortex over the rotor plane

All the equations derived and tested so far apply to a doubly infinite helical vortex. They give twice the velocities induced by a singly infinite (trailing) vortex only when $\theta = 0$. For non-zero θ, it will be shown below that the doubly infinite equations give $u(r, \theta) + u(r, -\theta)$ and $w(r, \theta) + w(r, -\theta)$ for a singly infinite vortex, and a further relation between the velocities is needed. Approximate relations for $u(r, \theta) - u(r, -\theta)$ and $w(r, \theta) - w(r, -\theta)$ can be derived from the Biot–Savart (BS) law for a line vortex.

Since the BS law provides a different method for determining the induced velocities, its relation to the KH equations, (1)–(4), is now briefly considered. The KH equations were derived from the velocity potential of a flow containing a doubly infinite helical vortex. The relationship with the BS law was analyzed by Morgan and Wrench (1965) and, more accessibly, by Boersma and Yakubovich (1998), whose Eq. 1 establishes the BS law as the "integral representation" of the series involving S_1 and S_3; see also Eq. (2.6) of Boersma and Wood (1999).

A straightforward application of the BS law gives

$$(u(r, \theta), w(r, \theta)) = \frac{\Gamma}{4\pi}\left(I_{u,BS}, I_{w,BS}\right) = \frac{\Gamma}{4\pi}\int_0^\infty \frac{\left(i_u(r, \theta), i_w(r, \theta)\right)}{d^3} d\beta,$$
(26)

where Γ is the vortex strength and β is the angle which is positive in the direction of positive θ. I_u and I_w, called the "influence functions," depend only on the geometry of the vortex. The limits indicate a singly infinite vortex so that $\beta = [0, \infty]$ for both θ and $-\theta$. The integrands contain
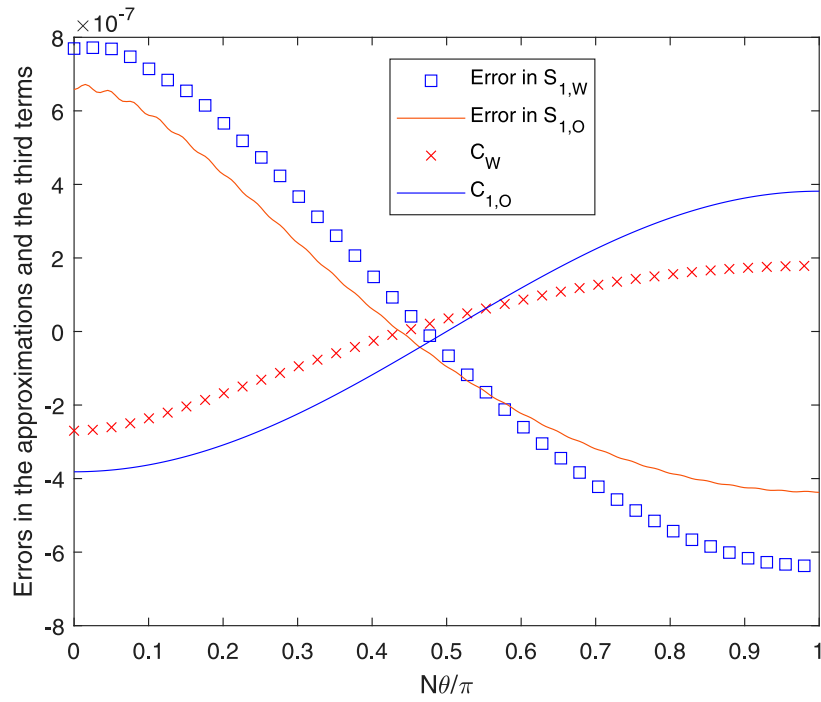
FIGURE 3
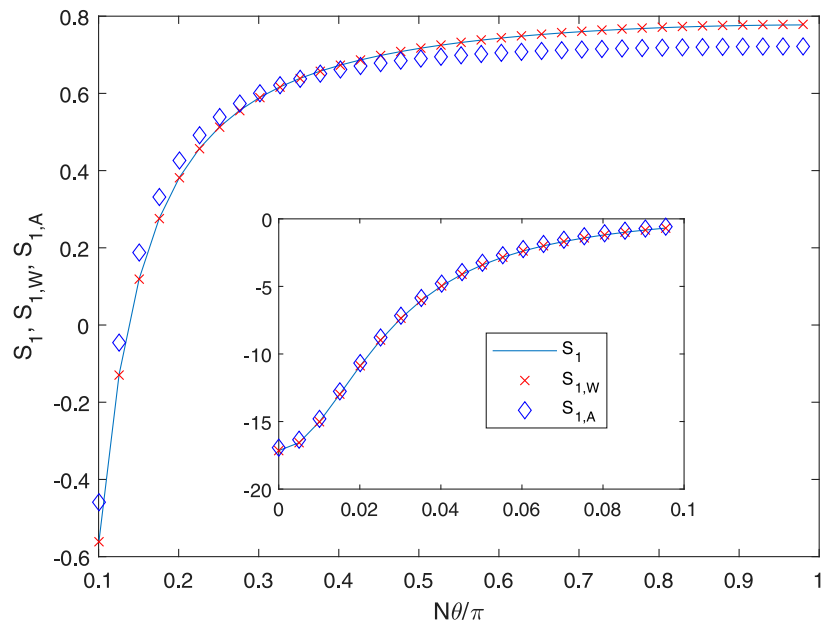Errors and third terms for the conditions in Figure 2.

FIGURE 4
S_1, $S_{1,W}$, and $S_{1,A}$ for $p = 0.1$, $r = 0.1$, and $t = 1$.

$$i_u(r,\theta) = t^2 - rt\cos(\beta - \theta) \quad \text{and}$$

$$i_w(r,\theta) = p(r - t\cos(\beta - \theta) - t\beta\sin(\beta - \theta)), \tag{27}$$

and the distance d is given by

$$d^2(r,\theta) = r^2 + t^2 - 2rt\cos(\beta - \theta) + p^2\beta^2. \tag{28}$$

The relationship between the doubly and singly infinite velocities can be seen from
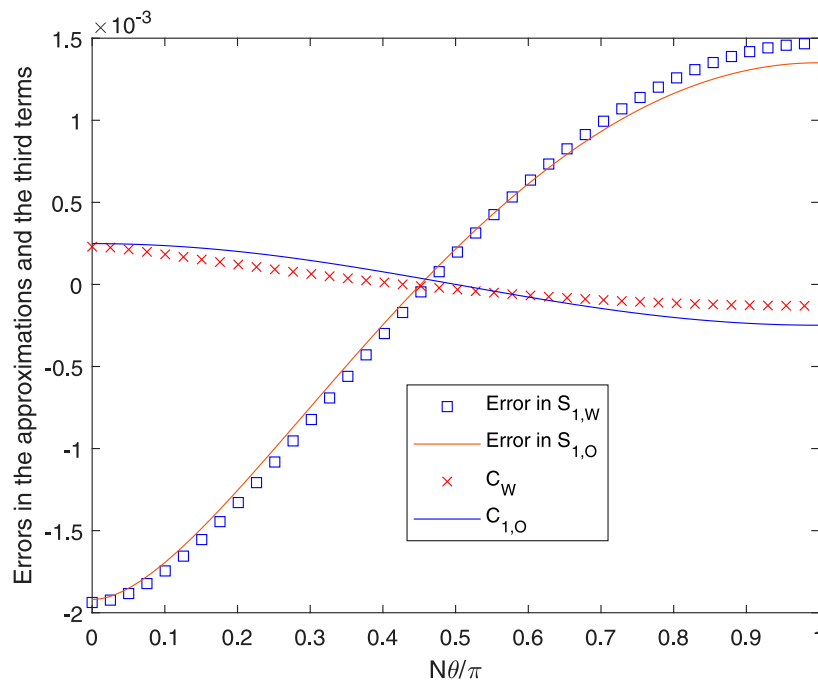
FIGURE 5
Errors and third terms for the conditions in Figure 4.

$$\int_{-\infty}^{\infty} \frac{i_u(r,\theta)}{d^3(r,\theta)} d\beta = \int_0^{\infty} \frac{i_u(r,\theta)}{d^3(r,\theta)} d\beta + \int_{-\infty}^0 \frac{i_u(r,\theta)}{d^3(r,\theta)} d\beta$$

$$= \int_0^{\infty} \frac{i_u(r,\theta)}{d^3(r,\theta)} d\beta + \int_0^{\infty} \frac{i_u(r,-\theta)}{d^3(r,-\theta)} d\beta$$

$$= I_{u,BS}(r,\theta) + I_{u,BS}(r,-\theta). \qquad (29)$$

It follows from (26) that

$$\int \frac{p i_u(r,\theta) + r i_w(r,\theta)}{d^3(r,\theta)} d\beta = \frac{p\beta}{\sqrt{t^2 + r^2 - 2rt\cos(\theta - \beta) + p^2\beta^2}}. \qquad (30)$$

By this extended version of helical symmetry, $w(r,\theta)$ can be obtained immediately from $u(r,\theta)$, so only the latter will be analyzed. Despite (30), the integrals for a helical vortex do not have closed-form solutions. Thus, the following approximation is made for the difference in the influence functions:

$$\Delta I_u = I_u(r,\theta) - I_u(r,-\theta) \approx \Delta I_{u,1} = \int_0^{2\theta} \frac{i_u(r,\theta)}{\left(r^2 + t^2 - 2rt\cos(\beta - \theta) + z^2\right)^{3/2}} d\beta, \qquad (31)$$

where $z = p\theta$. In words, the difference in the velocities is approximately that induced by a sector of a vortex ring of radius t located a distance $p\theta$ behind the control point. The approximation is sketched and further explained in Figure 6. In terms of β, measured from the intersection of the blue vortex and the green plane, the sector starts at $(t,0)$ and ends at $(t,2\theta)$. The integral in (31) has an analytic form that must be modified to give the correct asymptotic behavior as $r \downarrow 0$ for any t. In that limit, the integrand in (26) becomes independent

of θ, and so $\Delta I_u \to 0$. The result obtained using Mathematica is

$$\Delta I_{u,1} = \frac{2}{\sqrt{(r-t)^2 + z^2}} \left[\frac{r^2 - t^2 + z^2}{(r+t)^2 + z^2} E\left(\frac{\theta}{2}, \frac{-4rt}{(r-t)^2 + z^2}\right) \right.$$

$$\left. -F\left(\frac{\theta}{2}, \frac{-4rt}{(r-t)^2 + z^2}\right) \right]$$

$$+ \frac{4rt(r^2 - t^2 + z^2)\sin(\theta)}{\left(r^4 + 2r^2(z^2 - t^2) + (t^2 + z^2)^2\right)\sqrt{r^2 + t^2 + z^2 - 2rt\cos(\theta)}}$$

$$+ \frac{2t^2\theta}{(t^2 + z^2)^{3/2}}, \qquad (32)$$

where $E(.,.)$ and $F(.,.)$ are the incomplete elliptic integrals described in chapter 19 of DLMF (2023). The extra subscript was added to ΔI_u to denote the use of the full form of the integrals. Two more approximations with different additional subscripts are described below.

As for the doubly infinite results in Section 3, the tests on the accuracy of the approximations are restricted to $r < t$. A single vortex ($N = 1$) only will be considered, but some comments on the important cases of $N > 1$ are made below. The sum of the influence functions is

$$\Sigma I_u = I_u(r,\theta) + I_u(r,-\theta) \approx \Sigma I_{u,W} = \frac{t}{p^2} S_{1,W} \qquad (33)$$

when the $C-$ terms are ignored on the grounds that they are likely to be comparable to, or smaller than, the errors in using (32) for most turbine applications. The extra subscript in $I_{u,W}$ indicates that it was determined from Eq. 16. For comparison, the
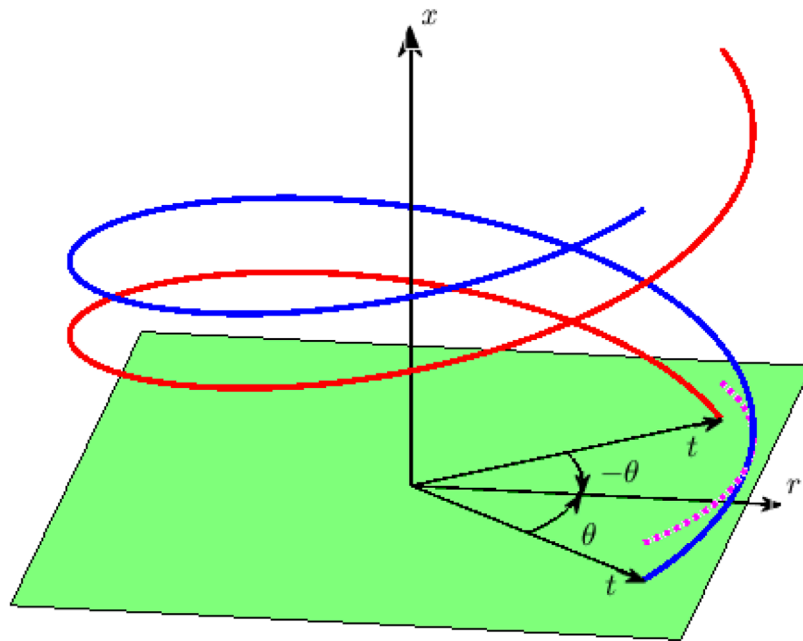
FIGURE 6
Difference in velocities induced by the blue and red singly infinite vortices anywhere along radius r is approximately the velocity induced by the vortex sector shown in dashed magenta. The sector of radius t spans $[-\theta, \theta]$ and is parallel to the green plane and distance $p\theta$ above it.

"exact" values of $I_{u,BS}(\theta)$ and $I_{u,BS}(-\theta)$ were determined by the numerical evaluation of the Biot–Savart integral for I_u in (26) using MATLAB's *integral* function with the default error settings, over $\beta = [0, \beta_{max}]$, from which $\Delta I_{u,BS}$ and $\Sigma I_{u,BS}$ follow. To the latter was added an analytic remainder approximating the integrals over $[\beta_{max}, \infty]$, as described in Appendix C. $\beta_{max} = 1000\pi$ was used for all results presented here. By varying β_{max}, this value was found to result in 6-figure accuracy for the results presented in the next section.

$\Sigma I_{u,BS}$ provides a check on the accuracy of $\Sigma I_{u,W}$ from (33). $\Delta I_{u,BS}$ will be used to show the errors in $\Delta I_{u,1}$ from Eq. 32, and further approximations using the simplification of the incomplete elliptic integrals described below. It is emphasized that the KH equations were found to give nearly identical results to those from the BS integration, but they are not considered further as they do not lead to an equation for ΔI_u.

Eq 33 is valid for all N, and it is unlikely that further simplification is possible. Eq. 32, however, has to be summed over N blades spaced $2\pi/N$ apart in a BEMT code, which raises three important considerations. First, the incomplete elliptic integrals are only partially periodic, as demonstrated by the small-modulus approximations of formulas (62:9:5) and (62:9:6) of Oldham et al. (2009):

$$F\left(\frac{\theta}{2}, m\right) \sim \frac{\theta}{2} + \frac{m}{4}\left(\theta - \frac{1}{2}\sin(\theta)\right) \text{ and } E\left(\frac{\theta}{2}, m\right) \sim \frac{\theta}{2} - \frac{m}{4}\left(\theta - \frac{1}{2}\sin(\theta)\right).$$
(34)

Thus, summation over N blades will not allow simple Kawada cancellation. Second, the integrals are computationally expensive to evaluate, so the accuracy of using (34) was tested. Surprisingly, the most accurate overall results came from ignoring the terms in m, leaving only $\theta/2$ for both F and E, which is very easy

for summing. Using (34), without any further modification to (32), leads to the second approximation to ΔI_u:

$$\Delta I_{u,2} = 2t\theta \left[\frac{t}{(t^2 + z^2)^{3/2}} - \frac{r+t}{((r+t)^2 + z^2)\sqrt{(r-t)^2 + z^2}} \right]$$
$$+ \frac{4rt(r^2 - t^2 + z^2)\sin(\theta)}{\left(r^4 + 2r^2(z^2 - t^2) + (t^2 + z^2)^2\right)\sqrt{r^2 + t^2 + z^2 - 2rt\cos(\theta)}},$$
(35)

which will be tested for accuracy along with $\Delta I_{u,1}$ from (32).

The third consideration is that the trigonometric term will simplify by Kawada cancellation when summed over N blades, but the presence of $\cos(\theta)$ in the denominator makes the result more complicated than that for the KH equations. Summing over N blades is equivalent to using the trapezoidal rule to approximate the integral of the periodic function:

$$\int_{\theta}^{\theta+2\pi} \frac{\sin(\beta)}{\sqrt{r^2 + t^2 + z^2 - 2rt\cos(\beta)}} d\beta$$
$$= \frac{1}{\sqrt{r^2 + t^2 + z^2}} \int_{\theta}^{\theta+2\pi} \frac{\sin(\beta)}{\sqrt{1 - a\cos(\beta)}} d\beta = 0,$$
(36)

where $a = 2rt/(r^2 + t^2 + z^2)$ satisfies $0 < a < 1$ for a BEMT code. Note that the integral is independent of θ, but generally, the trapezoidal approximation is not, even though Kawada cancellation always applies. In the limit of $a = 0$, however, the sum over N is zero for any θ. Thus, the sum of the trigonometric term, which is common to $\Delta I_{u,1}$ and $\Delta I_{u,2}$, tends to zero as $r \downarrow 0$ for $N > 1$. When $a = 1$, the integrand reduces to $\sqrt{2}\cos(\beta/2)$ for $\beta < 2\pi$ and $-\sqrt{2}\cos(\beta/2)$ for $\beta > 2\pi$, again giving a closed-form sum. The general form of

the sum is complicated and does not converge monotonically to zero at large N, probably because the complex variable form of the second integrand in (36) is not analytic when $a = 1$ (Trefethen and Weideman, 2014). When $a < 1$, the integrand is analytic, and the sums for large N are consistent with the exponential convergence of the trapezoidal rule for analytic functions that are periodic (Trefethen and Weideman, 2014). Nevertheless, the sum for small N when $a = 1$ appears to allow a simple approximation for $a < 1$ and the small values of N in a BEMT code:

$$\sum_{i=0}^{N-1} \frac{\sin\left(\theta + \frac{2\pi i}{N}\right)}{\sqrt{1 - \cos\left(\theta + \frac{2\pi i}{N}\right)}} = \sqrt{2} \sum_{i=0}^{N-1} \cos\left(\frac{\theta}{2} + \frac{\pi i}{N}\right)$$

$$= \sqrt{2}\left[\cos\left(\frac{\theta}{2}\right) - \cot\left(\frac{\pi}{2N}\right)\sin\left(\frac{\theta}{2}\right)\right], \quad (37)$$

provided $N\theta \leq 2\pi$. This suggests approximating the sum for any a as

$$\sum_{i=0}^{N-1} \frac{\sin\left(\theta + \frac{2\pi i}{N}\right)}{\sqrt{1 - a\cos\left(\theta + \frac{2\pi i}{N}\right)}} \approx \frac{\sin(\theta)}{\sqrt{1 - a\cos(\theta)}} - \sqrt{2}\cot\left(\frac{\pi}{2N}\right)\sin\left(\frac{\theta}{2}\right),$$

(38)

which is exact for $N = 1$ as $\cot(\pi/2) = 0$ and is accurate for other values of $N < 10$ approximately over a wide range of θ. Eq 37 shows that the sum becomes zero when $N = \pi/\theta$, which is large for small θ. Thus, the sum of the non-analytic function when $a = 1$ is algebraic rather than N times the exponential convergence of the trapezoidal rule when $a < 1$ and N is sufficiently large.

The convergence of the sum in (38) for $a < 1$ inferred from that of the trapezoidal rule shows that there are no sweep effects on the induced velocities for an actuator disc that is approached as $N \to \infty$, that is, much larger values than considered in the previous paragraph. Periodicity also requires $u(\pi) = u(-\pi)$, that is, $u(\theta) \to u(-\theta)$ as $\theta \to \pi$. This requirement is not satisfied by either (32) or (35), but this error is unlikely to be significant for moderate sweep and coning. As shown at the end of the next section, the error can be easily corrected.

5 Numerical tests of the singly infinite equations

Figure 7 plots the influence functions over $\theta = [0,\pi]$ for the conditions of Figure 2, except that now $N = 1$, and Figure 8 shows the various ΔI_u and ΣI_u. As expected from the previous results, Wrench's approximation for ΣI_u is very accurate at all θ. Both approximations for $I_u(\theta)$ are accurate at small θ when $I_u(\theta)$ is large in magnitude. Small θ is likely to occur frequently when the control point, r, is close to the vortex at t. There is, however, a very large difference between $I_u(\theta)$ and $I_u(-\theta)$, which remains close to zero for all θ. Only the exact influence functions asymptote to equality as $\theta \to \pi$, but the effect of the error in the others is likely to be small. The error is due almost entirely to the error at large θ in $\Delta I_{u,1}$ and $\Delta I_{u,2}$.

In Figure 9 for I_u and Figure 10 for ΔI_u and ΣI_u, r has been reduced to 0.1, which places it in the hub region where θ for $t = 1$ is likely to be larger than for $r = 0.99$ in a BEMT implementation. Now, $I_u(\theta)$ is nearly equal and opposite to $I_u(-\theta)$, and the typical magnitude has decreased substantially. Both approximations for I_u

differ from the exact solution at $\theta = \pi$, but the error may not be significant.

It is possible that the errors in ΔI_u are related to placing the vortex sector at the arbitrary location of $p\theta$ behind the control point. Changes to the position of the sector were investigated, but no overall improvement in accuracy was found, so all the present results were obtained using $z = p\theta$.

A simple way to restore the periodicity to I_u is to replace θ with $\sin(\theta)$ in Eq. 35. This gives the third approximation:

$$\Delta I_{u,3} = 2t\sin(\theta)\left[\frac{t}{\left(t^2 + z^2\right)^{3/2}} - \frac{r+t}{\left((r+t)^2 + z^2\right)\sqrt{(r-t)^2 + z^2}}\right.$$

$$\left. + \frac{2r\left(r^2 - t^2 + z^2\right)}{\left(r^4 + 2r^2\left(z^2 - t^2\right) + \left(t^2 + z^2\right)^2\right)\sqrt{r^2 + t^2 + z^2 - 2rt\cos(\theta)}}\right].$$

(39)

This approximation is not shown in Figures 7–9 to ensure their clarity. Figures 11, 12 plot the accuracy of $I_{u,i}$ for $i = 1, 2, 3$ for $t = 1.0, p = 0.1$, and $r = 0.99$ and 0.1, respectively. The "error" is $I_{u,BS} - I_{u,i}$, where $\Sigma I_{u,W}$ is used for all i. Overall, the third approximation is better than the second and is sometimes better than the first. As expected from $\Sigma I_{u,W}$ being substantially more accurate than $\Delta I_{u,i}$ for any i, the errors in $I_{u,i}(\theta)$ and $I_{u,i}(-\theta)$ are equal in magnitude and opposite in sign.

6 Discussion and conclusion

The main aim of this study was to extend the approximate methods for computing the induced velocities along straight, radial blades of horizontal-axis turbines and propellers, as described by Wood et al. (2021), to the whole rotor plane for blades that are swept. This extension also provides accurate approximations of the induced velocities for a swept or nonswept rotor anywhere in the plane of rotation. The basis for the analysis is the approximations derived by Wrench (1957) for the exact Kawada–Hardin (KH) equations for the velocity field of a doubly infinite vortex of constant pitch and radius. These equations involve infinite sums of products of Bessel functions and their derivatives, which cannot be evaluated quickly and accurately in many cases. The extension of the approximate equations is straightforward because the generalized sums described in Appendix A are not significantly more complicated than those needed to determine the velocities along straight and radial blades. Furthermore, blade element/momentum theory (BEMT) requires the induced velocities in the axial and circumferential directions. For all parts of the present analysis, there is a close connection between them, so only the axial velocity was considered in detail.

Comparison to the exact solutions showed the extended approximate equations are accurate. For some operating conditions, sufficient accuracy may be obtained using the first or $A-$ term. Two different third-order or $C-$ terms were used. The first extended the expansion of the Bessel functions by Wrench (1957) to the third order, and the second was the leading-order approximation to the alternative treatment of Okulov (2004) and Okulov and Sørensen (2020). The two expressions give similar results, but Okulov's expression is more accurate.
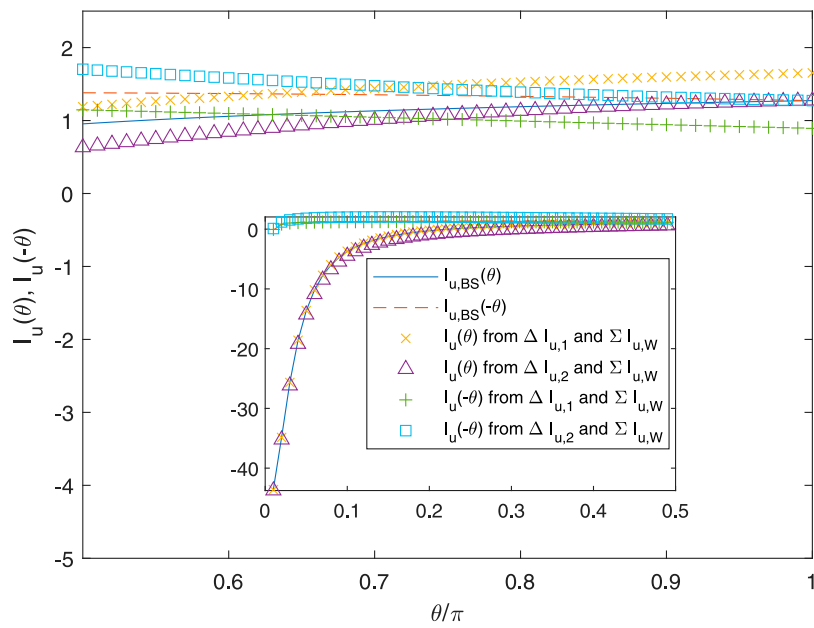
FIGURE 7
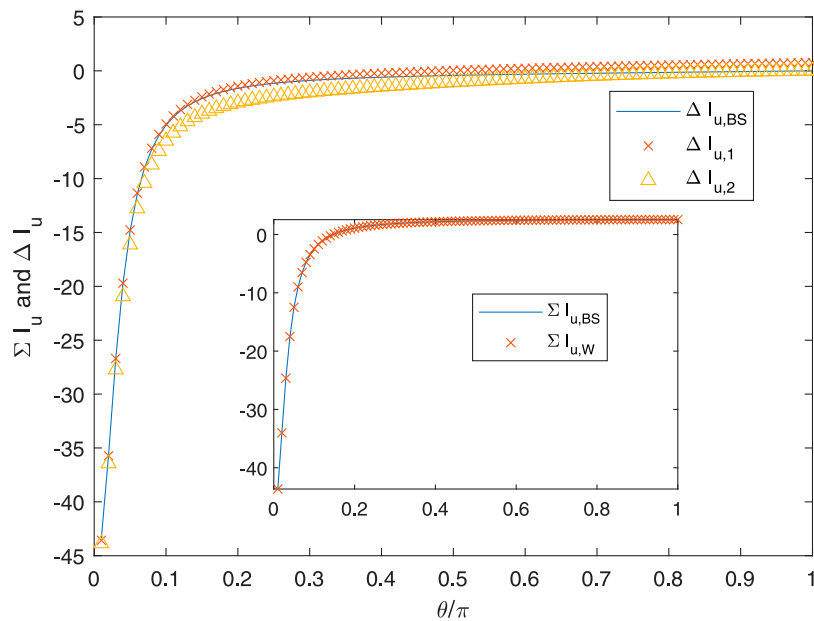Influence functions for $u(\theta)$ and $u(-\theta)$ for $N = 1, r = 0.99, t = 1.0,$ and $p = 0.1$.

FIGURE 8
ΣI_u and ΔI_u for $N = 1, r = 0.99, t = 1.0,$ and $p = 0.1$.

The application of the analysis in a blade element/momentum theory (BEMT) code must consider the differences between the doubly infinite results from the KH equations and the singly infinite vortices trailing from the junctions of the blade elements. For an angle θ between the origin of the trailing vortex and the control point, the KH equations give the sum of the velocities at $\pm\theta$. An additional, approximate equation for the difference in the velocities was derived from the Biot–Savart law. This equation contains incomplete elliptic integrals, which are computationally expensive to evaluate, so the first term in their low-modulus expansion was tested. This term was found to lead to accurate values of the induced velocity for small values of θ, but the accuracy reduced as θ approached π, which may well be applicable for the velocity induced in the hub region by the tip vortex.

The most interesting results from the previous section are those in Figures 7, 8 for small $|\theta|$, where $u(\theta)$ is much larger in magnitude than $u(-\theta)$. This suggests that the induced velocities when the blade is swept forward, whereby the tip is "ahead" of the
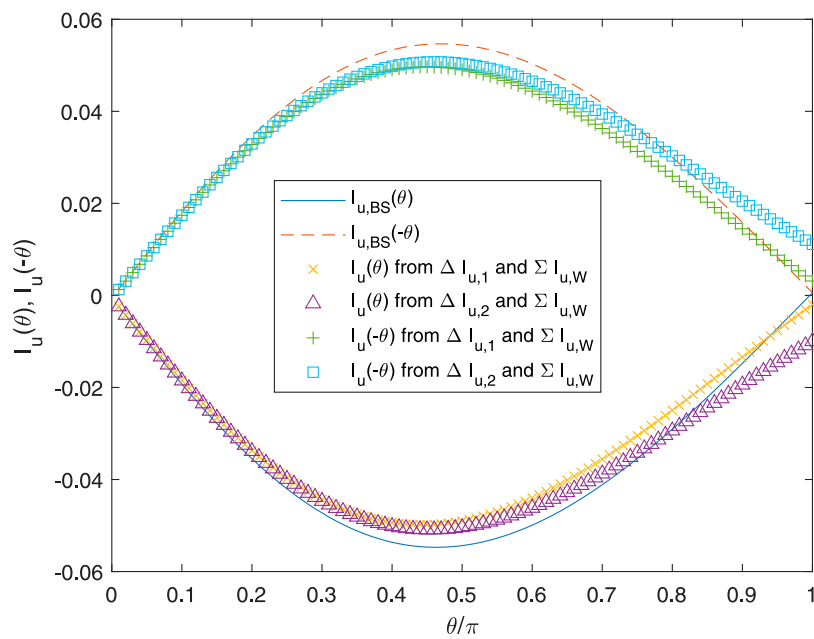
FIGURE 9
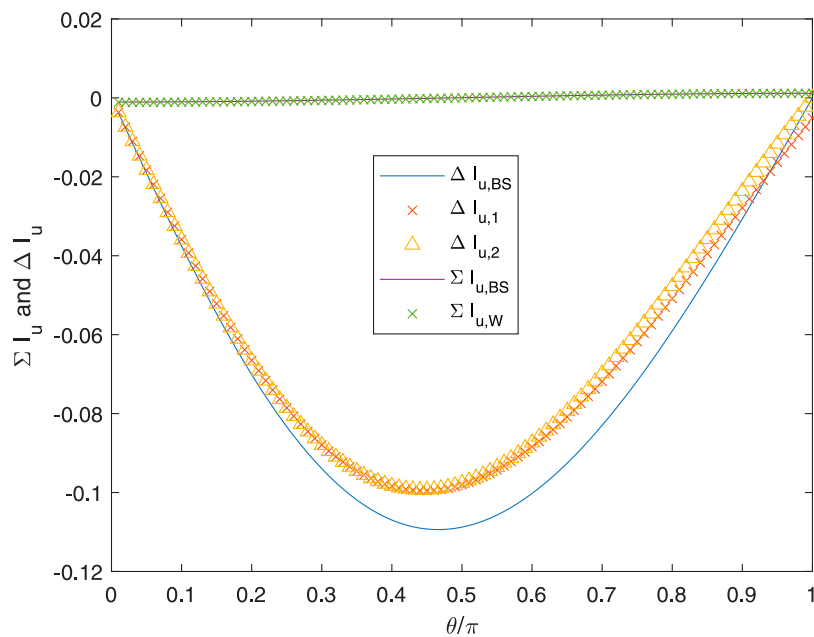Influence functions for $u(\theta)$ and $u(-\theta)$ for $N = 1, r = 0.10, t = 1.0$, and $p = 0.1$.

FIGURE 10
ΣI_u and ΔI_u for $N = 1, r = 0.10, t = 1.0$, and $p = 0.1$.

remainder of the blade, will be significantly different from those due to sweepback. Furthermore, the large magnitudes of $u(\theta)$ occur for small θ, suggesting that the LL representation of the blade may need revising to account for finite blade chords.

This analysis was developed for a single, swept blade, but it can be extended to multiple swept blades or to the more common situation of coned blades. The present equations require the control

point to have the same axial (windward) location as the start of the vortex, which is not the general situation for a coned rotor. The difference can be accommodated as follows. A vortex that starts behind (downwind of) a control point can be extended to the point's axial location. θ is now the angle between the extended vortex and the point, and the present analysis is applied to the trailing plus extended vortex. The velocity induced by the extension on
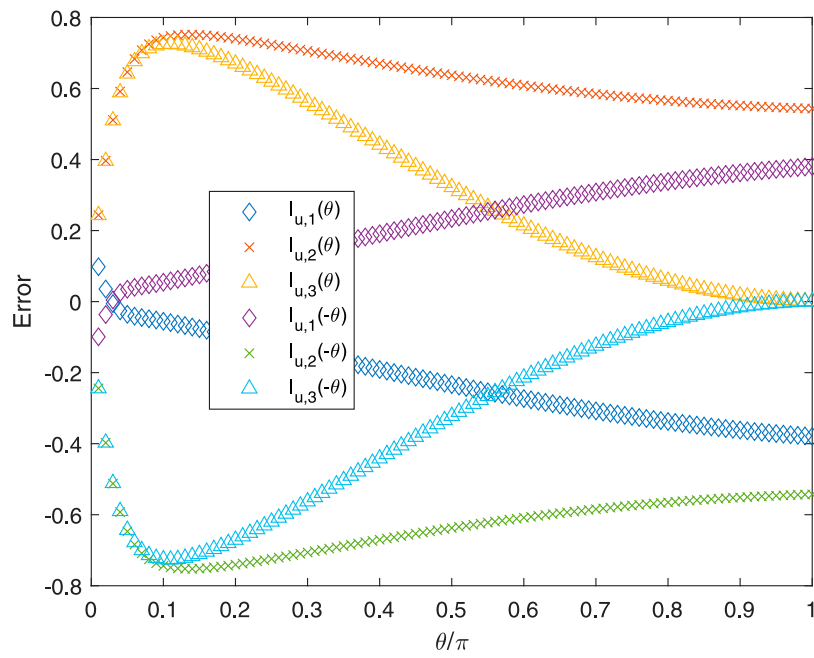
FIGURE 11
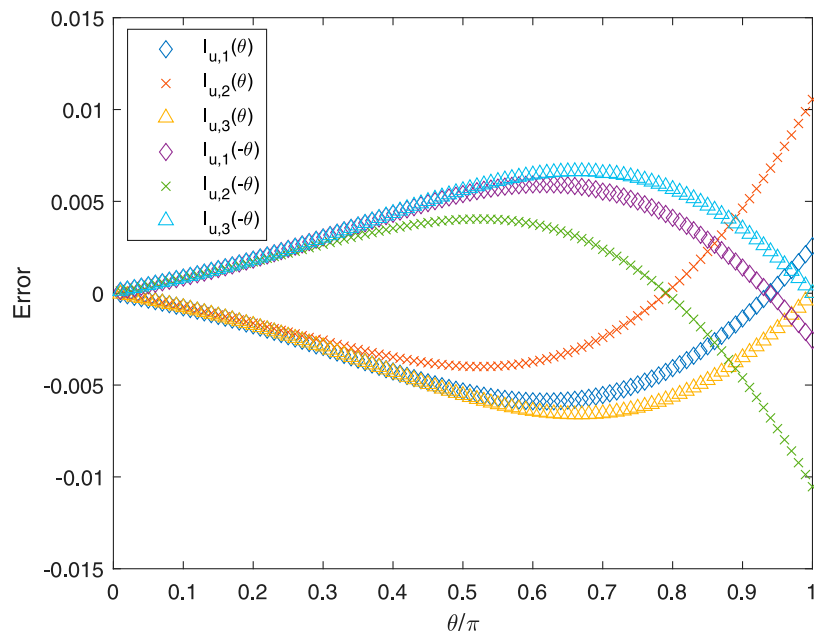Errors in the three approximations for I_u for $N = 1, r = 0.99, t = 1.0$, and $p = 0.1$.

FIGURE 12
Errors in the three approximations for I_u for $N = 1, r = 0.1, t = 1.0$, and $p = 0.1$.

its own can be determined using a simple modification to Eqs 32, 35 and then subtracted. A corresponding subtraction of a vortex segmentwould be the basis for computing the induced velocities when the control point lies behind the start of the vortex.

The further development of the present equations for use in a BEMT code for swept and coned rotors is currently underway. The computationally efficient extension of the equations for ΔI_u for an arbitrary number of blades is being developed together with

modifications to make $\Delta I_u(2\pi/N) = 0$ for any N. A major aim is to determine the necessity of the present method of determining the induced velocities in comparison to the much faster use of Prandtl's tip loss function.

Publisher's note

References

Bergmann, O., Möhren, F., Braun, C., and Janser, F. (2021). Aerodynamic analysis of swept propeller with BET and RANS. *Tech. Rep. DLR*.

Boersma, J., and Wood, D. (1999). On the self-induced motion of a helical vortex. *J. Fluid Mech.* 384, 263–279. doi:10.1017/s002211209900422x

Boersma, J., and Yakubovich, S. (1998). Solution to problem 97-18 ∗ : the asymptotic sum of a Kapteyn series. *SIAM Rev.* 40, 986–990.

DLMF (2023). in *NIST digital library of mathematical functions*. Editors Olver, F. W. J., Olde Daalhuis, A. B., Lozier, D. W., Schneider, B. I., Boisvert, R. F., and Clark, C. W. Release 1.1.10 of 2023-06-15. Available at: https://dlmf.nist.gov/.

Fritz, E. K., Ferreira, C., and Boorsma, K. (2022). An efficient blade sweep correction model for blade element momentum theory. *Wind Energy* 25, 1977–1994. doi:10.1002/we.2778

Gemaque, M. L., Vaz, J. R., and Saavedra, O. R. (2022). Optimization of hydrokinetic swept blades. *Sustainability* 14, 13968. doi:10.3390/su142113968

Gradshteyn, I., and Ryzhik, I. M. (2014). *Table of integrals, series, and products.* 8th edn. Academic Press.

Hardin, J. C. (1982). The velocity field induced by a helical vortex filament. *Phys. Fluids* 25, 1949–1952. doi:10.1063/1.863684

Kawada, S. (1936). Induced velocity by helical vortices. *J. Aeronautical Sci.* 36, 86–87. doi:10.2514/8.141

Kawada, S. (1939). *Calculation of induced velocity by helical vortices and its application to propeller theory.* Tech. Rep., 172. Tokyo: Aeronautical Research Institute.

Lehmer, D. H. (1944). Note on the computation of the Bessel function $I_n(x)$. *Math. Comput.* 1, 133–135. doi:10.1090/s0025-5718-44-99053-8

Li, A., Gaunaa, M., Pirrung, G. R., Meyer Forsting, A., and Horcas, S. G. (2022a). How should the lift and drag forces be calculated from 2-d airfoil data for dihedral or coned wind turbine blades? *Wind Energy Sci.* 7, 1341–1365. doi:10.5194/wes-7-1341-2022

Li, A., Pirrung, G. R., Gaunaa, M., Madsen, H. A., and Horcas, S. G. (2022b). A computationally efficient engineering aerodynamic model for swept wind turbine blades. *Wind Energy Sci.* 7, 129–160. doi:10.5194/wes-7-129-2022

Limacher, E. J., and Wood, D. H. (2021). An impulse-based derivation of the Kutta–Joukowsky equation for wind turbine thrust. *Wind Energy Sci.* 6, 191–201. doi:10.5194/wes-6-191-2021

Morgan, W. B., and Wrench, J. (1965). Some computational aspects of propeller design. *Methods Comput. Phys.* 4, 301–331.

Okulov, V. L. (2004). On the stability of multiple helical vortices. *J. Fluid Mech.* 521, 319–342. doi:10.1017/s0022112004001934

Okulov, V. L., and Sørensen, J. N. (2020). The self-induced motion of a helical vortex. *J. Fluid Mech.* 883, A5. doi:10.1017/jfm.2019.837

Oldham, K. B., Myland, J., and Spanier, J. (2009). *An atlas of functions: with equator, the atlas function calculator*. Springer.

Trefethen, L. N., and Weideman, J. (2014). The exponentially convergent trapezoidal rule. *SIAM Rev.* 56, 385–458. doi:10.1137/130932132

Wood, D., Okulov, V., and Vaz, J. (2021). Calculation of the induced velocities in lifting line analyses of propellers and turbines. *Ocean. Eng.* 235, 109337. doi:10.1016/j.oceaneng.2021.109337

Wood, D. H., and Hammam, M. M. (2022). Optimal performance of actuator disc models for horizontal-axis turbines. *Front. Energy Res.* 10. doi:10.3389/fenrg.2022.971177

Wrench, J. (1957). The calculation of propeller induction factors. Tech. Rep. Tech. Rep. 1116. David Taylor Model Basin.

Appendix A: Summation of the cosine series

This appendix provides a derivation of the sums that appear in the $A-$, $B-$, and $C-$ terms for S_1 in the main text. The derivation for the corresponding terms for S_3 is so similar that it is not shown.

Starting with the infinite sum of the geometric series,

$$\sum_{m=1}^{\infty} z^m = z/(1-z), \qquad (A1)$$

for any $|z| < 1$, substituting for $z = U_W \exp(iN\theta)$, and separating the real and imaginary parts, gives

$$\sum_{m=1}^{\infty} U_W^m \cos(mN\theta) = \frac{U_W(\cos(N\theta) - U_W)}{1 + U_W^2 - 2U_W \cos(N\theta)}, \qquad (A2)$$

whose right side is the first term in Eq. 16, and

$$\sum_{m=1}^{\infty} U_W^m \sin(mN\theta) = \frac{U_W \sin(N\theta)}{1 + U_W^2 - 2U_W \cos(N\theta)}. \qquad (A3)$$

Integrating (A3) with respect to $N\theta$ gives

$$\sum_{m=1}^{\infty} \frac{U_W^m \cos(mN\theta)}{m} = -\frac{1}{2} \log\left(1 + U_W^2 - 2U_W \cos(N\theta)\right). \qquad (A4)$$

For $\theta = 0$, (A2) and (A4) lead to Eqs (13) and (14), respectively, and for non-zero θ, to (16) and (17). A similar integration of Equation (A2) results in

$$\sum_{m=1}^{\infty} \frac{U_W^m \sin(mN\theta)}{m} = -\frac{N\theta}{2} - \tan^{-1}\left(\frac{(1 + U_W)\tan(N\theta/2)}{U_W - 1}\right). \qquad (A5)$$

A further integration with respect to $N\theta$ would give the sums in the $C-$ terms in the text, but the indefinite integral was long and unwieldy, so an alternative treatment was developed.

From the definition of the polylogarithm function, $\text{Li}_s(z)$:

$$\sum_{m=1}^{\infty} \frac{U_W^m \cos(mN\theta)}{m^s} = \frac{1}{2}\left[\text{Li}_s\left(U_W e^{iN\theta}\right) + \text{Li}_s\left(U_W e^{-iN\theta}\right)\right], \qquad (A6)$$

as described in chapter 25 of DLMF (2023). Since $\text{Li}_s(z)$ is available in languages such as Mathematica and MATLAB, it should be possible to extend Wrench's expansion to any order. The present analysis, however, is restricted to $s = 2$. $Li_2(.)$ is called the "dilogarithm."

Appendix B: The circumferential integrals for S_1 and S_3

As a check on the derivation of $S_{1,W}(N\theta)$, its integral over the 2π region of periodicity was determined. A similar analysis was done for

the $S_{3,W}(N\theta)$, but the results are not shown in the interests of brevity. Since $A-$, $B-$, and $C-$ terms are not directly related, the integral of each term in (16) must be zero. For the $A-$ term in (16),

$$\int_{-\pi}^{\pi} \frac{U_W \cos(N\theta) - U_W^2}{1 + U_W^2 - 2U_W \cos(N\theta)} d(N\theta)$$

$$= -\frac{1}{2}\int_{-\pi}^{\pi}\left(1 - \frac{1 - U_W^2}{1 + U_W^2 - 2U_W \cos(N\theta)}\right)d(N\theta). \qquad (B1)$$

Now $U_W < 1$ for $S_{1,W}$, so the indefinite integral is given by formula (2.556.2) of Gradshteyn and Ryzhik (2014). Over $[-\pi, \pi]$, the integral is zero.

For the $B-$term in $S_{1,W}$, which is multiplied by A, it is convenient to integrate over $[0, 2\pi]$. It is necessary to show that the following integral is zero:

$$\int_0^{2\pi} \log\left(1 + U_W^2 - 2U_W \cos(N\theta)\right) d(N\theta), \qquad (B2)$$

which is by formula (4.224.15) of Gradshteyn and Ryzhik (2014).

Since

$$\int \left[\text{Li}_s\left(U_W e^{iN\theta}\right) + \text{Li}_s\left(U_W e^{-iN\theta}\right)\right] dN\theta$$

$$= \frac{i}{N}\left[\text{Li}_{s+1}\left(U_W e^{iN\theta}\right) + \text{Li}_{s+1}\left(U_W e^{-iN\theta}\right)\right], \qquad (B3)$$

C_W must integrate to zero over $[0, 2\pi]$. The same is obviously true for Eqs (24) and (25).

Appendix C: The analytic remainders for the Biot−Savart integrals

When $p\theta \gg (r + t)^2$, d in (28) can be approximated as $d \approx p\beta$, and the remainder, $R_u(\theta, \beta_{max})$, is given by

$$R_u\left(\theta, \beta_{max}\right) = \int_{\beta_{max}}^{\infty} \frac{i_u(r, \theta)}{d^{3/2}(r, \theta)} d\beta \approx \int_{\beta_{max}}^{\infty} \frac{i_u(r, \theta)}{(p\beta)^{3/2}} d\beta, \qquad (C1)$$

which was evaluated using *Mathematica*. The leading-order terms for large $p\beta$ give

$$R_u\left(\theta, \beta_{max}\right) + R_u\left(-\theta, \beta_{max}\right) \approx \frac{t^2}{p^3 \beta_{max}^2} \qquad (C2)$$

and

$$R_u\left(\theta, \beta_{max}\right) - R_u\left(-\theta, \beta_{max}\right) \approx 0, \qquad (C3)$$

independently of θ.

Nomenclature

β	Vortex angle
ΔI_u	$I_u(\theta) - I_u(-\theta)$
Γ	Circulation
λ	Tip speed ratio
ΣI_u	$I_u(\theta) + I_u(-\theta)$
θ	Angle between the vortex and control point
A	Leading term in the approximate solution for S_1 and S_3, Eq. 8
B	Second term in the approximate solution for S_1 and S_3, Eq. 11
C	Third term in the approximate solution for S_1 and S_3, Eqs 20, 23, 24
c_r	Term defined in Equation (8)
c_t	Term defined in Equation (8)
$C_{1,O}$	Okulov's equation for C, Eqs (23) and (24)
C_W	Third term in Wrench's expansion, Eq. 20
I_u	Influence function for induced u
m	Index for the summation of trigonometric terms
$m_{\max}$	Upper limit on m for s specified accuracy
N	Number of blades
p	Pitch of the helical vortex
r	Radius of the point at which velocity is required
S_1	Series defined by Eq. 5
S_3	Series defined by Eq. 6
$S_{1,W}$	Wrench's approximation to S_1, Eq. 13
$S_{3,W}$	Wrench's approximation to S_3, Eq. 14
t	Radius of the helical vortex
u', w'	Azimuthally dependent axial and circumferential velocities, respectively
u, w	Axial and circumferential velocities, respectively
U_W	Term in Wrench's approximation, Eq. 8
x	Streamwise coordinate